Chapter 2

Materials by Design: Multiscale Molecular Modelling for the Design of Nanostructured Membranes

Erik Laurini, Maurizio Fermeglia* And Sabrina Pricl

Molecular Simulation engineering (MoSe) Laboratory, University of Trieste, Department of engineering and Architecture (DeA), piazzale europa 1, 34127 Trieste, Italy *e-mail: maurizio.fermeglia@units.it

2.1 Introduction

Advanced materials are essential for economic security and human well- being, with applications in industries aimed at addressing challenges in clean energy, national security, and human welfare. Despite this paramount importance, the development of a new advanced material can take 20+ years from its initial discovery to the market. Accelerating the pace of discovery and the deployment of advanced materials are therefore crucial to achieving global competitiveness in the 21st century. In 2011, the Federal Government of the United States launched the Materials Genome Initiative (MGI) with an investment of over $250 million in new R&D and innovation infrastructures to boost the use of advanced materials in existing and emerging industrial sectors in the United States.[1] The basic idea of the MGI is the integration

of three different tools, namely simulations, experiments, and big data (Figure 2.1). In the MGI strategy, simulations and experiments are coupled and optimised in order to provide reliable data under different conditions and for different properties: they are tightly integrated with slight overlapping to define the relative ranges of

Membrane Engineering for the Treatment of Gases: Gas-separation Issues with Membranes, Volume 1
Edited by Enrico Drioli, Giuseppe Barbieri and Adele Brunetti

Published by the Royal Society of Chemistry, www.rsc.org

uncertainties. In particular, simulations are used to complement experiments in a range of conditions under which experiments are hard to carry out, as well as to speed up the procedure of characterisation of new materials with different formulations. All the relevant results obtained by both tools are stored in databases (big data), which in turn are queried by specific analytical tools capable of obtaining the necessary information from the data and supplying them to the industrial sectors.

The MGI philosophy for the design of new materials is also central to the concept of Industry 4.0, in which digitalisation is going to deeply convert the way new products and new processes are developed.[2] Industry 4.0 is mainly based on the use of big data, cloud computing, internet-of-things, and simulation tools, coupled with robotics and sensors able to acquire data, analyse them, and give feedback to actuators aiming at enhancing the efficiency of production processes.

Membrane technology, and particularly nanocomposite Membrane Technology (nMT), with its multiple areas of application and its incredible potential in different fields is one of the industrial sectors getting strong benefits from the MGI approach.[3] This is mainly due to the plethora of different systems with different properties that may be obtained by mixing a polymer with nanoparticles, as well as the general low cost of the process and raw materials.

Figure 2.1 Materials Genome Initiative: a materials innovation infrastructure combining simulation with experiments and digital data.

In this chapter, we will concentrate on one of the tools of the MGI, the computational tool, explaining in particular the concept of multiscale molecular modelling, which is aptly suited for the design, optimisation, and property prediction of nanocomposite membranes.[4] We will also present and discuss a comparison of predicted data with real experiments, thereby using two main features of the MGI initiative and ultimately proving the reliability of computational tools in this specific field.

polymer nanocomposite membranes are complex systems consisting of

polymeric matrices in which nano-objects are dispersed in order to obtain specific gas transport and separation properties. These materials are also generally known as polymer nanocomposites (pnCs) and display structure features that span several length scales, from the Å level of the individual backbone of a single chain to the mesoscopic system morphology, reaching far into hundreds of nanometres. In addition, the time scales of the characteristic dynamic processes relevant to such different nanostructured material properties span a wide range, from femtoseconds to milliseconds, or even seconds or hours in glassy materials or large-scale ordering processes (*e.g.* phase separation in blends). Unfortunately, no single model or simulation algorithm can cover such an interval of length and time scales; therefore, the seamless integration of many different models, each suitable for the description of the chemistry and the physics at a given time and/or length scale, is required.

This concept indeed constitutes the pillar of multiscale molecular modelling and simulation, that is, the bridging of length and time scales by linking computational methods to ultimately predict the macroscopic properties and behaviour of complex systems from fundamental molecular processes.[5–8] In fact, despite the advances made in the modelling and prediction of structural, thermal, mechanical, and transport properties of materials at the macroscopic (continuum) level, a tremendous uncertainty still remains on how to predict many properties of industrial interest for materials exhibiting peculiar structures at the nanoscale. Thus, the idea of performing simulations of materials across several characteristic length and time scales, starting from fundamental physical principles and experimental data, has an obvious appeal as a tool of potential great impact on technological innovation and material design.[9]

To sum up, the advantages of considering multiscale molecular modelling include, among others, the following:

- the reduction of the product development time by alleviating costly trial-and-error iterations;
- the reduction of product costs through innovations in materials, products, and process design;
- the reduction of the number of costly, large-scale experiments;
- the increase of product quality and performance by providing more accurate predictions in response to material design requirements and loads; • the support provided to conceive and develop entirely new materials.

Multiscale molecular modelling can be applied to almost all materials whose properties depend on their nano-structure or micro-structure. Accordingly, this contribution is not conceived as a thorough presentation of all the current state-of-the-art multiscale molecular modelling approaches.[7,10–14] Rather, the selected examples presented in this overview reflect the authors' own research interests, and are by no means exhaustive. nevertheless, it is our hope that they can serve as inspiration for further developments in this exciting branch of science.

2.2 Multiscale Molecular Modelling: General Concepts

The use of computer modelling techniques has experienced a rapid expansion in both materials and life sciences in the last 15 years, with the number of relevant articles indexed in Scopus and ISI Web of knowledge more than tripling between 2004 and 2016 in comparison to the preceding decade. Accordingly, computational modelling is now a well-established technique in virtually all areas of mainstream materials science, including polymers, ceramics, semiconductors, metals, and of course membranes.

Many important driving forces have boosted the use of computer molecular modelling and simulations in materials science. probably the most important one is the availability of (relatively) inexpensive commodity processing power, driven in part by Moore's law, which, in its original form, related to the doubling of the transistor density in integrated circuits every 18 months. In practice, this has led to a rapid decrease in the unit price of CpUs (Central processing Units), GpUs (Graphical processing Units), physical memory, and hard disk space, as machines suitable for scientific calculations have found their way onto the mass market. parallel to hardware improvement, a plethora of free and commercially available integrated modelling software packages now exists, a selection of notable examples includes Gaussian® (mainly for quantum mechanics calculations); AMbeR and nAMD (for atomistic simulations); Materials Studio®, Culgi, GRoMACS, and LAMMpS (for both atomistic and mesoscale simulations); and Digimat and AbAQUS® (for continuum, *i.e.*, finite element, calculations). by definition, multiscale molecular modelling entails the application of computational techniques at two or more different length and time scales, which are often, but not always, dissimilar in their theoretical character due to the variation in scale. A distinction is made between the *hierarchical approach*, which involves running separate models with some sort of parametric coupling, and the *hybrid approach*, in which models are run concurrently over different spatial regions of a simulation. The relationships between the different categories of methods commonly used in the multiscale modelling hierarchy are shown in Figure 2.2. Although some techniques have been

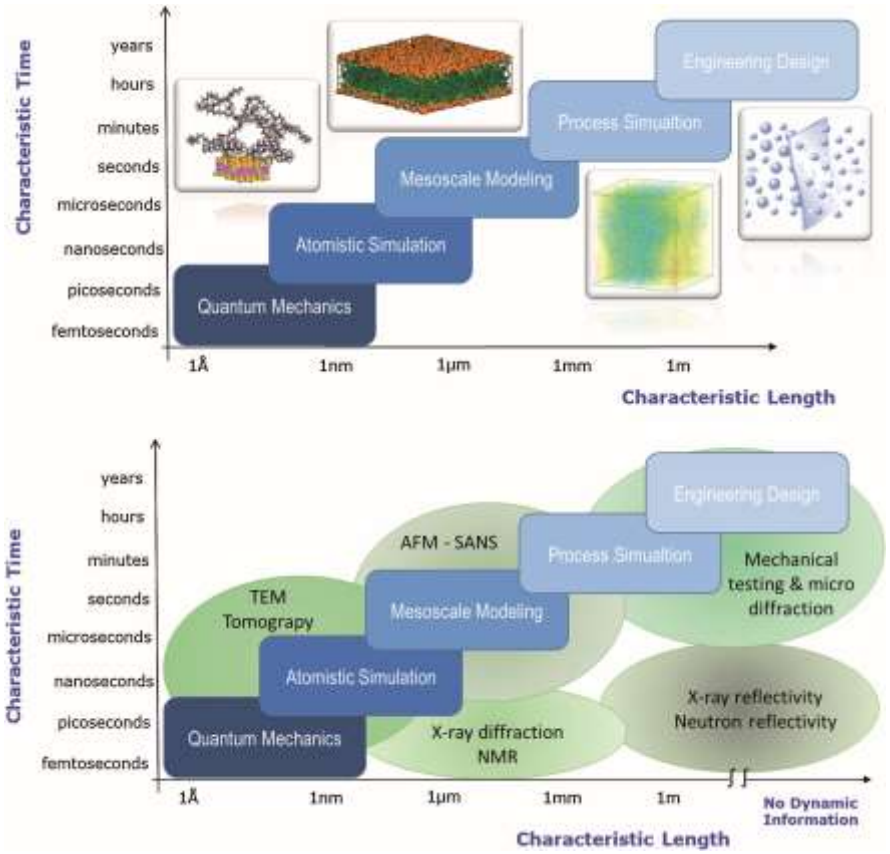

Figure 2.2 (Top) The hierarchy of multiscale molecular modelling techniques, showing the approximate range of temporal and spatial scales covered by the different categories of methods. Areas of overlap permit "mapping" or "zooming" from one scale to the next, which is often required for parameterisation of higher scale methods or for obtaining a finer scale resolution of selected parts of a large system. (bottom) experimental and theoretical tools for the characterisation and modelling of polymer-based nanocomposites, plotted over their respective time and length scale domains of applicability. The experimental methods include X-ray diffraction, nuclear magnetic resonance (nMR), transmission electron microscopy (TeM), tomography, atomic force microscopy (AFM), small-angle neutron scattering (SAnS), small-angle X-ray scattering (SAXS), mechanical testing, X-ray reflectivity, and neutron reflectivity.

known for a long time and are currently widely used (*e.g.*, molecular dynamics (MD) and Monte Carlo (MC) methods), other such as mesoscale simulation (MS) and some more advanced methods for accelerating atomistic simulations are not as common yet, and require more advanced experience and specialised background in the field.

In the context of materials simulations shown in Figure 2.2 (top panel), four characteristic time and length levels can be envisaged before reaching the last step, *i.e.*, engineering design:[16]

1. T he *quantum scale* (10^{-10}–10^{-9} m and ~10^{-12} s), in which nuclei and electrons are the main players, and their quantum-mechanical states dictate the interactions between atoms. The possibility of obtaining data describing the structural and electronic features of the system being considered and of taking into account effects associated with the rupture and formation of chemical bonds in molecules, changes in electron configurations, and other similar phenomena are the main advantages of methods working at the quantum scale.
2. T he *atomistic scale* (10^{-10}–10^{-7} m and 10^{-12}–10^{-6} s). In atomistic simulations, all atoms are explicitly represented or, in some cases, small groups of atoms are treated as single sites referred to as pseudo- or united atoms. The potential energy in the system is estimated using a number of different classes of interactions (collectively known as force fields), typically consisting in: (i) bonded interactions, including bond-length (stretch) potentials, bond-angle (bend) potentials, torsion (twist) potentials, and cross-terms; and (ii) non-bonded interactions, mostly comprising Coulomb interactions and dispersion forces.
3. T he *mesoscopic scale* (10^{-9}–10^{-1} m and 10^{-6}–10 s). In these methods, a molecule is usually treated with a field description (field-based model) or microscopic particles (particle-based model) that incorporate the molecular details implicitly. Therefore, they are able to simulate phenomena on length and time scales currently inaccessible by classical atomistic approaches. At the simplest mesoscopic level, a polymer system may be modelled by a phenomenological expression for the free energy (field-based approach). For example, the Flory–huggins or Landau free energies of mixing may be used to model aspects of polymer mixtures. In such models, the details of the system are incorporated into, *e.g.*, the Flory parameter and the monomer segment mobility. Such phenomenological expressions are equivalent to truncated expansions of a more complicated free energy expression. Instead, in particle-based models, the fluid is portrayed as a collection of point particles that represent lumps of fluid containing many molecules or segments of chains, termed beads. The interaction between beads is considered mesoscopic because the internal degrees of freedom of the fluid elements are ignored and only their centre-of-mass motion is resolved.
4. T he *macroscopic scale* (10^{-3}–10 m and 10–10^{3} s). At this level, constitutive laws govern the behaviour of the physical system, which is considered as a continuous medium, ignoring discrete atomic and molecular structures and their influence on the overall system behaviour. The basic assumption then consists in representing a heterogeneous material as an equivalent homogeneous one. A medium is called a continuum if its volume contains an apparent continuity of material mass over the physical scale of the problem of interest. In general, this requires the domain of interest to be several orders of magnitude larger than the length scale of the elemental components. All the mathematical functions (*e.g.*, velocity or displacement fields) used to describe the state of the system are continuous, except possibly at a finite number of interior surfaces separating regions of continuity. Stress and strain tensors may be split into isotropic and deviatory parts, allowing the prediction of the behaviour of the medium under both static and dynamic loadings with separate descriptions of the material constitutive behaviour under hydrostatic and non-hydrostatic circumstances.

At each length and timescale, well-established and efficient computational approaches have been developed over the years to handle the relevant, underlying phenomena. To treat electrons explicitly and accurately at the lower scale, electronic models based on quantum mechanical (QM) methods can be employed. QM methods have undergone enormous advances in the last decades, enabling the simulation of systems containing several hundred atoms with good accuracy.[15] For material properties at the atomic level, MD and MC simulations are usually performed employing classical interatomic potentials, which can often be derived from QM calculations.[17,18] Although not as accurate as QM methods, classical MD and MC simulations are able to provide insight into atomic processes involving considerably large systems.[19] At the mesoscopic scale, the atomic degrees of freedom are not explicitly treated, and only large-scale entities are modelled (that is, the agglomeration of atoms called *beads*, obtained through a coarse-graining procedure, *vide infra*). Mesoscale models are particularly useful for studying the behaviour of polymers and soft materials. They can model even larger molecular systems, but with a commensurate trade-off in accuracy. Typical results of mesoscale simulations are the morphology of matter in the nanometre–millimetre range under specific conditions of temperature, composition, and shear. Various simulation methods have been proposed to study the mesoscale structures of polymer-based materials, the most common being brownian Dynamics, Dissipative particle Dynamics, Lattice boltzmann, time-dependent Ginzburg–Landau theory, and Dynamic Density Functional Theory.[20–25] eventually, it is possible to transfer the simulated mesoscopic structure to finite element modelling (FeM) tools to calculate the macroscopic properties for the systems of interest.[26,27]

Whatever the multiscale protocol developed, it is important to be able to compare the calculated results with experimental evidence at each of the scales in which a computation is performed. Fortunately, the experimental methods available now allow this comparison along the entire multiscale procedure, as shown in the bottom panel of Figure 2.2. experimental tools and methodologies available at different time and length scales allow not only checking of the validity of the simulations but also feeding of data to the big data repository in the framework of the MGI mentioned above.

In summary, being the ultimate goal of multiscale modelling the prediction of the macroscopic behaviour of an engineering process from first principles by adopting a sequential simulation pathway, information at a small (fine) scale is first computed and passed onto a model at a larger (coarser) scale. This procedure leaves out (*i.e.*, coarse grains) all the degrees of freedom pertaining to the smaller scale, which is considered to be in equilibrium.[14,28–32]

Two ingredients are required to construct a successful sequential multiscale model: first, it is necessary to have an *a priori* complete knowledge of the fundamental processes involved at the smallest scale. This knowledge or information can then be employed to model the system at successively coarser levels. Second, it is necessary to acquire a reliable strategy to incorporate the lower-scale information into the coarser scales. This is often accomplished by phenomenological theories, which contain few key parameters, the values of which are determined from the information at the lower scales.

This *message-passing* approach can be performed in sequence for multiple-length scales. The vital attribute of the sequential approach is that the simulations at the higher levels critically depend on the completeness and correctness of the information gathered at the lower levels, as well as on the efficiency and reliability of the model at the coarser levels. To obtain first principles-based results for macroscale systems, a sufficient degree of overlap between each simulation scale and the finest description must be ensured, so that all input parameters and constitutive laws at each level of theory can be determined from fundamental theories. equally important, these relations must be invertible so that the results of coarse level simulations can be used to suggest the best choices for finer level parameters, which, in turn, can be employed to formulate new choices of material composition and structure.

The problem for polymers is that the method of coarsening the description from atomistic to mesoscale/mesoscale to continuum is not as obvious as it is in going from electrons to atoms.[6] In other words, the coarsening from QM to MD relies on basic principles that can be easily generalised in a method and in a procedure, while the coarsening at higher scales is system specific. Multiscale simulation poses, in some sense, greater challenges for polymer materials than for seemingly more complex systems, such as metals and ceramics, due to the larger range of length and time scales that characterise macromolecules. In this respect, for example, Doi developed a suite of simulation tools that model polymers at the molecular and mesoscale level.[33] Although each tool performs calculations using only one technique, the output from one level can be used directly as input for another, allowing an offline bridging of length and time scales. To achieve what he and others refer to as *seamless zooming*, namely the ability to spawn higher resolution simulations using more detailed methods where needed, will require additional theoretical and computational advances. Along similar lines, off-line multiscale simulations of polymer nanocomposites using coarse-grained MD, the mesoscopic time dependent Ginsburg–Landau theory, and macroscopic continuum finite element techniques have been carried out. Significant advances in uniquely mapping atomistic models of polymers onto coarse-grained models have been made in recent years, in some cases providing nearly exact quantitative agreement between the two models for certain quantities.[34–36]

Scale integration in specific contexts in the field of polymer modelling can be done in different ways. Any ‘computational recipe’ for passing information from one scale to another (upper) scale is based on the definition of multiscale modelling, which considers *objects* that are relevant at that particular scale, disregard all the degrees of freedom of the smaller scales, and summarise those degrees of freedom by some representative parameters.

All approaches are initially based on the application of a force field (FF) that transfers information from quantum chemistry to the atomistic simulation. From the atomistic simulation to the mesoscale model, essential features of the system have to be maintained while reducing the degree of freedom.

So far, the features chosen for the reproduction by coarse-grained models have been mainly structural, thermodynamic, or both, with structure prevailing over the other.[37] This linking through the mesoscale, through which we can describe the

microstructure, is probably the most challenging step toward the development of reliable first principles methods for practical material design applications.

Among the possibilities for achieving seamless zooming multiscale simulations in the field of polymer-based nanocomposites, we present and discuss here one strategy that has proven to yield accurate and reliable results for many different systems of industrial interest.[38] According to this multiscale computational recipe, four sequential steps need to be performed, as follows:

i. QM calculations are employed (when required) to derive specific (and, hence, highly accurate) force fields, that is, material energy functions (interatomic potentials) comprising the functional forms and parameter sets used to calculate the potential energy of a system of atoms or coarse-grained particles in molecular mechanics/molecular dynamics simulations. ii. having chosen the appropriate FF for the system under consideration (either already available in the literature or derived *ad hoc* in the previous step), fully atomistic MD simulations are performed to retrieve fundamental structural and energetical information at the molecular level.

iii. The data gathered in point (ii) are mapped into the corresponding structural and energetical input parameters required to run simulations at the mesoscopic level.

iv. The main output from point (iii), *i.e.*, the mesoscopic morphologies and density distributions of the system, are finally used as the input for finite element calculations and macroscopic property predictions.

In the remaining part of this chapter, we will present and discuss in detail the application of such hierarchical multiscale molecular modelling approach to the prediction of gas permeation and diffusion in nanostructured polymeric membranes constituted by different thermoplastic polyurethanes (TpUs) as the matrix and spherical titania nanoparticles (Tio_2) as the nanofiller.

2.3 Multiscale Simulation Prediction and Experimental Validation of Gas Permeation Enhancement in Different Thermoplastic Polyurethane (TPU)/TiO_2 Nanocomposite Membranes

Generally speaking, dispersing impermeable particles in polymers results in a decrement of the gas permeability in the corresponding polymer nanocomposite (pnC) with respect to the pristine polymeric matrix.[39] however, for pnCs, this rule has its own exceptions. For instance, chain packing in glassy polymers can be disturbed/disrupted by the presence of nanofillers, leading to an increased free volume in the polymeric phase.[40,41] This, in turn, results in an increased gas permeability.[42–46] In other words, the presence of void spaces at the polymer–particle

interface or between particles in the case of nanofiller-imperfect dispersion (*i.e.*, nanoparticle aggregation) causes the permeability of nanocomposites to increase with respect to the relevant unfilled polymers. Accordingly, in the remaining part of this chapter, we will present the application of a combined experimental/computational investigation on polymer nanocomposite systems for which this "anomalous" behaviour is observed, that is, thermoplastic polyurethane (TpU) membranes loaded with spherical, nanosized Tio_2 particles.

TpUs are nanophase-separated diblock copolymers, constituted by a so-called hard (crystalline) phase (hF) – prototypical components being 4,4′-methyl-diphenylisocyanate (MDI) and the chain extender 1,4-butanediol (bDo) – interspersed within a soft (amorphous) phase (SF) – most commonly a polyester or polyether block. The morphology of TpU matrices is inherently multiscale, being characterised by the presence of nano, meso, and microstructures, which, in turn, are crucial for the application properties of the final material. Specifically, the low glass transition temperature of the TpU soft phase and the crystallinity of the hard phase make this class of polymers amenable for the fabrication of mechanically stable membranes for gas transport and separation. nonetheless, many attempts have aimed at maximising the membrane performance by varying the molecular components of TpUs, where the pristine polymeric matrix suffers from a trade-off between permeability and selectivity.[47] one efficient way to supersede these limitations consists in the dispersion of inorganic nanoparticles (*e.g.*, silica, alumina, graphene, layered silicates, *etc*.) at the nanometre level within the TpU polymers.[48–50] owing to its properties, titanium dioxide has recently drawn considerable attention in the manufacturing of polymer-based nanocomposite membranes for different uses.[51] Tio_2 exists in three different crystalline forms: rutile (the most stable phase), anatase, and brookite. of the three, anatase nanoparticles can be obtained in sizes smaller than 5 nm, and this feature, coupled with other interesting qualities, renders this nanofiller particularly attractive in the field of polymer-based nanocomposite membranes.[52] Accordingly, in this work, we adopted a multiscale simulation/experimental approach to analyse the effect of different contents of nano-Tio_2 (*i.e.*, 0, 2.5, 5, 7.5, and 10% by weight) on the o_2, n_2, Co_2, and Ch_4 transport and selectivity of TpU matrices characterised by different chain extenders. Specifically, all TpU considered were based on soft segments constituted of polytetramethylene-glycol of molecular weight 1000 (TeG1000) and 4,4′-methyl-diphenylisocyanate (MDI) as the hard phase. ethylene glycol (eG), 1,4-butanediol (bDo), 1,6-hexanediol (hDo), and 1,10-decanediol (DDo) chain extenders were used to complete the conversion of pre-polymers into the final TpUs. For all polymers, the molar ratio of TeG1000, MDI, and chain extender was 1 : 3 : 2.

2.3.1 Experimental and Computational Information

All TpU matrices were synthesised *via* a two-step bulk polymerisation technique,[53] while an organic–inorganic hybrid technique was employed *in situ* to generate Tio_2 nanoparticles in the TpUs.[52] TpU/Tio_2 nanocomposite membranes were obtained *via* solution casting at room temperature. The Tio_2 content (average nanoparticle diameter was 3 nm as measured by TeM) was calculated by thermogravimetric analysis (TGA) and found to be in excellent agreement with the nominal values

(indicating almost 100% conversion), in agreement with previous reports.[52] Gas permeability (*P*) values and diffusion coefficients (*D*) were measured using the vacuum time-lag method.[54]

Computer-based predicted values of gas permeability and diffusivity in the different TpU matrices were obtained *via* application of the multiscale molecular simulation procedure outlined in Section 2.2. The atomistic structures of all TpU chains were built and optimised according to Laurini *et al.*[55] To generate spherical anatase Tio_2 nanoparticles at the atomistic level, a sphere of 3 nm diameter was cut out of a larger lattice constructed using the corresponding lattice parameters (space group: *I*41/amd; *A*: 3.875 Å; *C*: 9.514 Å, *Z* (number of atoms per cell) = 4). MD simulations in canonical (nVT) ensemble yielded the final nanoparticle structure at room temperature. Its validity was checked by comparing experimental/predicted X-ray structures of anatase Tio_2 nanoparticles. next, one Tio_2 nanoparticle was embedded in each TpU matrix and the corresponding nanocomposite was first subjected to geometry optimisation and then to extensive constant pressure-constant temperature (npT) MD simulations. The equilibrium density of each TpU/Tio_2 nanocomposite membrane was obtained from the volumes averaged over the entire equilibrium-stage MD runs. To determine the gas diffusion coefficients, *N* molecules of each gas were inserted at random within an equilibrated TpU matrix model extracted at a point along the corresponding equilibrated MD trajectory; the relevant systems were then subjected to npT simulations[56] and the corresponding *D* values for each gas were obtained *via* the well-known einstein relationship:

$$D = \frac{1}{6N} \lim_{t \to \infty} \frac{d}{dt} \sum_{i=1}^{N} \left\langle \left| R_i(t) - R_i(0) \right|^2 \right\rangle \tag{2.1}$$

where *N* is the number of diffusing molecules, $R_i(t) - R_i(0)$ stands for the vector distance travelled by gas *i* over the time interval *t*, and $\langle |R_i(t) - R_i(0)| \rangle^2$ represents the time-averaged mean square displacement of gas *i*.

The morphology of each TpU/Tio_2 nanocomposite membrane and the density distribution of the nanocomposite components (to be used later in gas permeability predictions, *vide infra*) were predicted at the mesoscopic level *via* Dissipative particle Dynamics (DpD).[22] According to DpD theory, the essential intra- and inter-molecular interactions taking place between all the molecular actors of the mesoscopic simulations are expressed by the values of the conservative parameter a_{ij}. This quantity accounts for the underlying chemistry of the system under consideration. In this work, we employed a well-validated strategy that correlates the interaction energies estimated from lower scale (atomistic MD) simulations to the mesoscale a_{ij} parameter values.[11–14,18,30–32,35,38,57–63] Following and adapting this computational recipe, the interaction energies of all the pnC system components estimated from MD simulations were rescaled onto the corresponding mesoscale segments. The last step of the proposed multiscale simulation procedure corresponds to the prediction of the gas permeability for the considered polymer nanocomposites as a function of the filler loading. To this purpose, finite element (Fe) calculations were performed. Thus, the *P* values were estimated by mediating each corresponding property of the

nanoparticle core (*i.e.*, the pure nanoparticle property) and of the interphase (as obtained by running fixedgrid calculations using the mesoscopic density distribution input information) for the corresponding weight fractions. As mentioned previously, the density profiles of each component obtained from mesoscale simulations were used as input for gas permeability calculations. Finally, the bulk properties of each pure component of the diverse pnCs constituted the last information necessary to run the FeM calculations.[14]

2.3.2 Results

A typical example of enhanced gas transport in polymeric nanocomposite membranes is reported in Figure 2.3 for pnCs obtained by dispersion of Tio_2 nanoparticles into TpU chains formed by TeG1000, MDI, and chain extenders of different length (eG, bDo, hDo, and DDo).

As seen from Figure 2.3, the experimental permeability is an increasing function of the Tio_2 content for all considered gases. The same trend is observed in computer simulations, with permeability predictions in quantitative agreement with the measured values. In detail, the enhancement factors are greater than one for all gases, indicating higher permeabilities in the case of nanocomposites compared to those of the corresponding pristine matrices. Interestingly, at each given nanoparticle concentration, the enhancement factor (eF) was found to increase with the molecular volume of the permeating gas (Figure 2.3), that is $eF_{Ch4} > eF_{n2} > eF_{o2} > eF_{Co2}$, in agreement with the kinetic diameter d_k of the corresponding gases (*i.e.*, $d_{k,Ch4}$ (3.80 Å) > $d_{k,n2}$ (3.64 Å) > $d_{k,o2}$ (3.46 Å) > $d_{k,Co2}$ (3.30 Å)).[64] Moreover, the presence of progressively longer chain extenders in the TpU polymer contributes to the gas permeability enhancement for all the gases under consideration. This is apparent when comparing the corresponding panels in Figure 2.3. Thus, for instance, focusing on the highest nanoparticle loading (*i.e.*, 10 wt%) as a proof of concept, it is seen that, going from eG to DDo, the permeability eF increases from 2.02 (*simulated value 2.19*) to 2.96 (*2.89*) for o_2 (panels A–D),

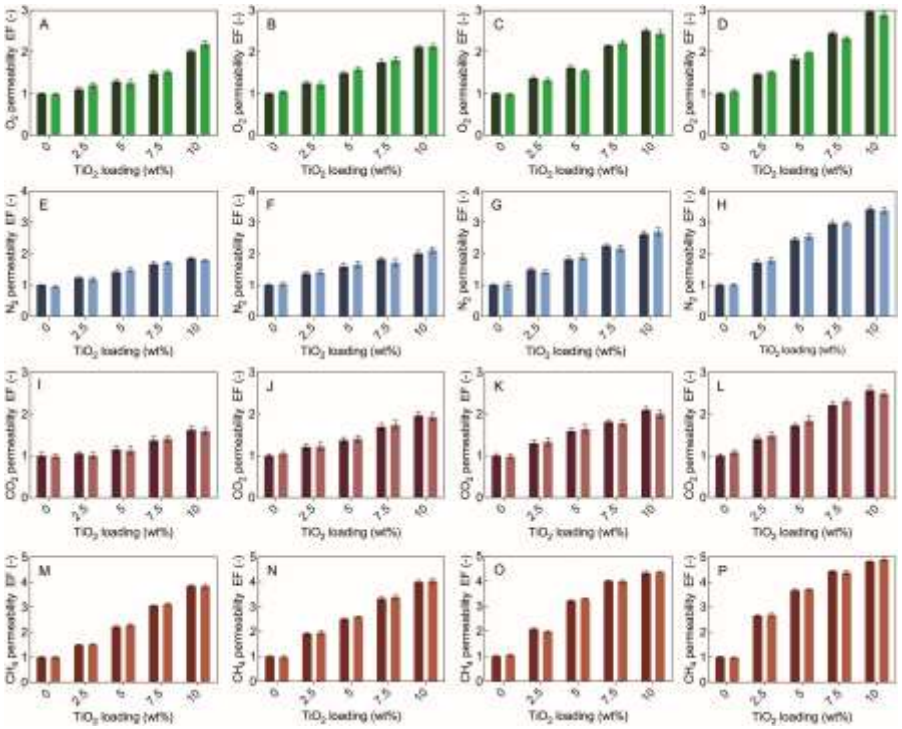

Figure 2.3 effect of the chain extender on the gas permeation eF for n_2 (A–D), o_2 (e–h), Co_2 (I–L), and Ch_4 (M–p) in TpU/Tio_2 pnCs as a function of the nanoparticle loading. TpU composition: (A, e, I, and M), TeG1000MDI-eG; (b, F, J, and n), TeG1000-MDI-bDo; (C, G, k, and o), TeG1000MDI-hDo; and (D, h, L, and p), TeG1000-MDI-DDo. Dark colour bars: experimental data; light colour bars: computational data. experiments and simulations were run in triplicate. experimental data are unpublished results from the authors.

from 1.85 (*1.80*) to 3.42 (*3.38*) for n_2 (panels e–h), from 1.62 (*1.58*) to 2.57 (*2.49*) for Co_2 (panels I–L), and from 3.85 (*3.83*) to 4.82 (*4.91*) for Ch_4 (panels M–p). Such behaviour is a clear indication that, for each TpU composition, the dependence of the permeability of larger gaseous molecules on the Tio_2 nanofiller concentration is a steeper increasing function than that describing the behaviour of smaller gases in the same polymeric nanocomposite membranes. Table 2.1 shows this trend for the TeG1000-MDI-bDo system as an example. Moreover, such different degrees of gas permeability enhancement further lead to a reduction of the o_2/n_2 and Co_2/Ch_4 selectivity with the increasing nanoparticle content (Table 2.1).

The current literature reports several cases in which the addition of impermeable nanoparticles to polymeric matrices augments their gas permeability instead of exerting a negative effect on this technologically important transport property.[41,42,46,47,50,65] Different arguments have been adopted to explain this "anomalous" behaviour, such as defective chain packing around the spherical nanoparticles, leading to an increased free volume in the polymeric matrix and, hence, enhanced gas diffusion, a solubility increase mechanism due to the interaction between the penetrant gas and the nanofillers, and the so-called nano-gap hypothesis,

according to which, due to the poor compatibility between the nanoparticle surface and polymer chains, these cannot get in tight contact with the nano-inclusions, thus forming a narrow gap around the nanoparticles themselves. As a consequence, the gas diffusion pathway becomes shorter and, hence, the diffusivity and permeability increases.[41] besides these explanations, other authors have postulated that the interstitial cavities enclosed in nanoparticle aggregates might also be responsible for the increased gas permeability.[66] Finally, in other cases, the increased gas permeability has been attributed to macroscopic defects at the polymer–filler interface that allow fast gas transport.[67]

Simulated mesoscale morphologies fully support the evidence that the interstitial cavity mechanism is not operative in all the TpU-based nanocomposite membranes considered in this work, as shown in Figure 2.4 for the TeG1000-MDI-bDo/Tio_2 (10 wt%) system as an example. Indeed, the image confirms that the Tio_2 nanoparticles are dispersed individually within the TpU matrix with almost no aggregates being observed.

Table 2.1 experimental/*computational* gas permeability and selectivity of TeG1000MDI-bDo TpU/Tio_2 nanocomposite membranes as a function of the nanofiller concentration. experimental data are unpublished results from the authors. All data standard deviations are within 10%.

	Gas permeability *P* (barrer)				Gas selectivity (−)	
Tio_2 (wt%)	o_2	n_2	Co_2	Ch_4	o_2/n_2	Co_2/Ch_4
2.5	2.83/*2.70*	0.64/*0.70*	37.6/*39.9*	3.82/*3.80*	4.42/*3.86*	9.84/*10.5*
5	3.37/*3.49*	1.02/*1.01*	42.6/*46.1*	4.97/*5.05*	3.30/*3.45*	8.57/*9.13*
7.5	3.96/*3.93*	1.23/*1.16*	52.6/*56.9*	6.61/*6.59*	3.22/*3.38*	7.96/*8.63*
10	4.79/*4.64*	1.55/*1.40*	60.9/*63.1*	7.94/*7.86*	3.09/*3.31*	7.67/*8.03*

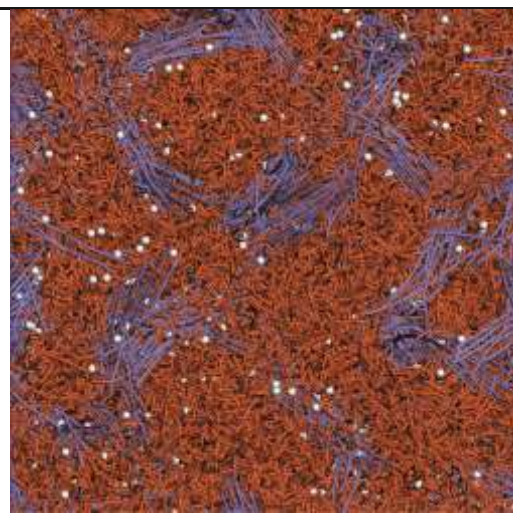

Figure 2.4 Mesoscale simulated morphology of the TeG1000-MDI-bDo TpU/Tio_2 (10 wt%) nanocomposite membrane. orange: TpU soft phase; purple: TpU hard phase; white, Tio_2 nanoparticles.

Second, should macroscopic defects be present, gas transport dominated by a pore flow mechanism would occur, and the gas selectivity of the polymer membrane would tend toward the knudsen limit:

$$K_{A/B} = \sqrt{\frac{MW_B}{MW^A}} \tag{2.2}$$

where MW_A and MW_b are the molecular weight of gas A and b, respectively; or to the poiseuille limit:

$$P_{A/B} = \frac{}{\mu_A} \tag{2.3}$$

in which μ_A and μ_b are the viscosity of the gases. As can be seen in Tables 2.1 and 2.2, however, for the systems under investigation, the o_2/n_2 and Co_2/Ch_4 selectivities are neither at their knudsen limits (0.94 and 0.60, respectively) nor at their poiseuille limits (0.86 and 0.69, respectively).

In a third instance, it might be recalled here that different gas transport mechanisms are reflected as diffusion coefficient values differing by orders of magnitude. As shown in Figure 2.5, all the simulated/experimental diffusion coefficients *D* for all TpU/Tio_2-based nanocomposite membranes analysed in this work are of the order of 10^{-7} cm^2 s^{-1}, a prototypical value for solution-diffusion driven mechanisms; in contrast, knudsen diffusion is characterised by *D* values four orders of magnitude smaller.[68]

The same figure also reveals that the presence of longer chain extenders in TpU contributes to increasing the values of *D* for a given gas at a given wt% of

Table 2.2 experimental/*computational* gas permeability and selectivity of TeG1000MDI TpU/Tio_2 (10 wt%)-based nanocomposite membranes as a function of the chain extender length. All data standard deviations are within 10%. Data for calculations of $K_{A/b}$ (eqn (2.2)) and $P_{A/b}$ (eqn (2.3)): MW_{o2} = 32; MW_{n2} = 28; MW_{Co2} = 44; MW_{Ch4} = 16; μ_{o2} = 0.0205 cp; μ_{n2} = 0.0177 cp; μ_{Co2} = 0.0150 cp; μ_{Ch4} = 0.0103 cp at 25 °C.

	Gas permeability *P* (barrer)				Gas selectivity (−)	
Chain extender	o_2	n_2	Co_2	Ch_4	o_2/n_2	Co_2/Ch_4
eG	4.44/*4.71*	1.39/*1.27*	48.6/*49.5*	6.22/*5.95*	3.19/*3.71*	7.81/*8.32*
bDo	4.79/*4.64*	1.55/*1.40*	60.9/*63.1*	7.94/*7.86*	3.09/*3.31*	7.67/*8.03*
hDo	6.30/*6.00*	2.13/*2.25*	68.3/*74.4*	9.57/*10.0*	2.96/*2.67*	7.14/*7.44*
DDo	8.02/*7.62*	3.01/*2.94*	84.8/*81.8*	12.2/*11.3*	2.66/*2.59*	6.95/*7.24*

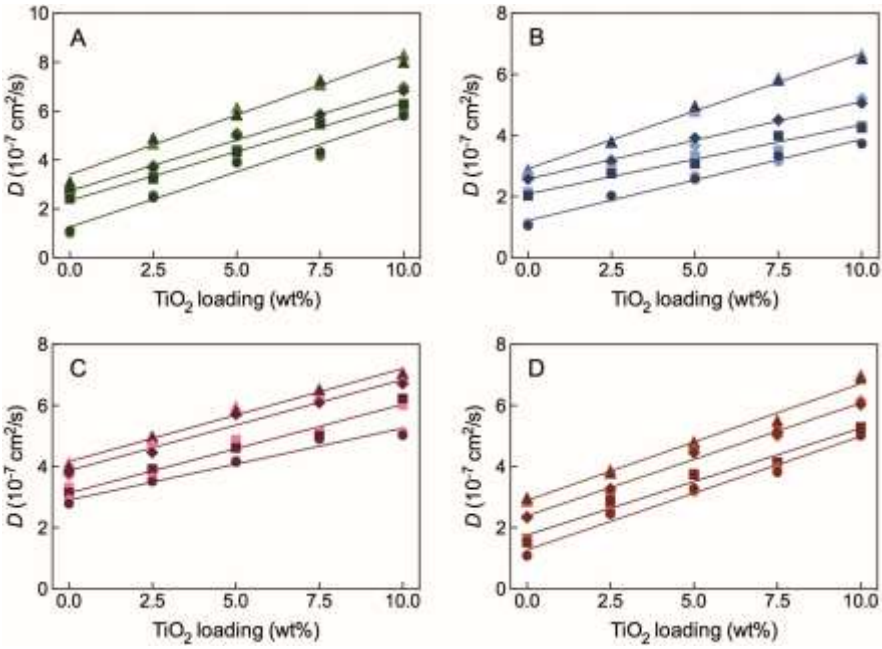

Figure 2.5 Simulated (darker colour symbols)/experimental (lighter colour symbols) diffusion coefficients *D* for (A) o_2, (b) n_2, (C) Co_2, and (D) Ch_4 in TeG1000-MDI TpU/Tio_2 nanocomposite membranes as a function of the nanoparticle concentration and chain extender length. Symbol legend: circles, eG; squares, bDo; diamonds, hDo; and triangles, DDo. Lines are data fitted with linear regression. experiments and simulations were run in triplicate. Data standard deviation (within 10%) not shown for clarity. experimental data are unpublished results from the authors.

Tio_2, without altering the dependence of *D* on the nanofiller concentration. Thus, gases travel somewhat faster in TpU/Tio_2 nanocomposite membranes having DDo as the chain extender than in those incorporating eG in their hard phase.

The estimation/measurement of *D*, together with that of the permeability *P*, allows to obtain the gas solubility values *S* in the same membranes, *via* the standard relationship: $P = D \times S$, as illustrated in Figure 2.6 for TeG1000-MDIbDo/Tio_2 nanocomposite membranes as an example.

As seen from this figure, the solubility coefficients in all the TpU/Tio_2 nanocomposite membranes considered decreases from Co_2 to n_2, following the order: $S_{Co2} > S_{Ch4} > S_{o2} > S_{n2}$. This trend correlates with the condensability characteristics of these gases, which, in turn, are directly proportional to the gas critical temperature T_c (T_{cCo2} = 304.12 k, T_{cCh4} = 190.56 k, T_{co2} = 154.58 k, and T_{cn2} = 126.26 k).

In aggregates, all these computational/experimental results exclude the possibility of macroscopic defects at the polymer–nanoparticle interface, but also the presence of membrane defects due to experimental casting problems because of poor casting practice, leaving an increased free volume due to Tio_2 interference with the chain packing as the plausible cause of the counter-intuitive gas transport in these TpU-based nanocomposite membranes. To this purpose, it is important to recall here that TpU chains are inherently poorly flexible, and become even more so upon solvent

evaporation during membrane casting. Accordingly, whilst in solution, the polymer chains are still flexible enough to wrap the nano-Tio_2 particles; once the solvent has evaporated, the polymer chains are subjected to very high stress levels and, as such, cannot pack efficiently around the spherical

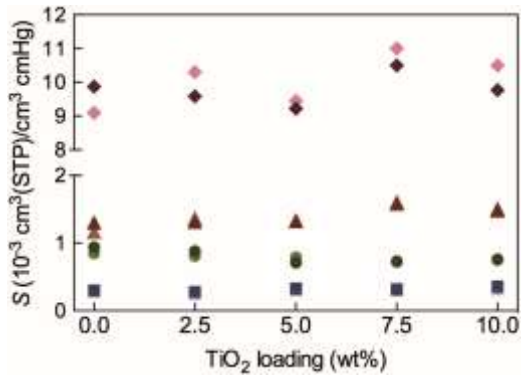

Figure 2.6 experimental/computational solubility coefficients (as derived from the fundamental relationship: $S = P/D$) for o_2 (circles), n_2 (squares), Co_2 (diamonds), and Ch_4 (triangles) in TeG1000-MDI-bDo/Tio_2 nanocomposite membranes as a function of the nanoparticle concentration. Dark colour: experimental data; light colour: computational data. Data standard deviation (within 10%) not shown for clarity. experimental data are unpublished results from the authors.

nano-inclusions (Figure 2.4). This, in turn, gives rise to a considerable free volume region at the polymer–Tio_2 interface. Such "low-density" interfaces offer significantly lower resistance to pathways for gas diffusion than the bulky polymer matrix.

To verify this hypothesis and estimate the relevant free volume fraction within each TpU/Tio_2 nanocomposite membrane, the density of each system was measured/predicted. The idea underlying density measurements/ simulations is that, for an "ideal" binary polymer/nanoparticle system, the system density should be additive; accordingly, the corresponding value of density ρ_{add} can be easily calculated from the densities of each system component (*i.e.*, ρ_p and ρ_n) and the nanocomposite composition, according to eqn (2.4):[69]

$$\square_{add} \square \frac{w_N / \square_N}{w_N / \square_N \square w_P / \square_P} \qquad (2.4)$$

in which w_n and w_p are the weight fraction of the nanofiller and polymer, respectively. on the other hand, in the presence of polymer–nanoparticle interactions ultimately resulting in a relative alteration of the nanocomposite component properties, the effective system density ρ_{eff} should deviate from ideality. Under the assumption that such deviations from density additivity are related to the polymer only, positive variations of ρ_{eff} can be generally ascribable to a compacting action exerted by the nanoparticles on the polymer chains, whilst negative variations are indicative of the

structural compaction of the polymer/nanofiller system being less efficient than expected. obtaining experimental density values in nanocomposite systems is not trivial, and requires delicate measurements by, *e.g.*, gas displacement picnometry.[52] Accordingly, given the excellent agreement between the experimental and simulated data obtained for all the transport properties illustrated above, density values for all TpU/Tio_2 nanocomposite membranes were predicted computationally. Interestingly, all nanocomposite membranes considered in this work show significant deviation from ideality, as indicated in Figure 2.7(A) for TeG1000-MDI-bDo systems as a proof of concept. The simulated density values ρ_{eff} are considerably lower than those corresponding to the additive model ρ_{add} (eqn (2.4)), the deviation increasing with the increasing Tio_2 content in the membrane.

As such, the data in Figure 2.7 indicate that these systems are characterised by the presence of a considerable number of voids either within the polymeric matrix or at the polymer–nanofiller interface, thereby providing support to the hypothesis that the dispersion of Tio_2 nanoparticles interfere with the efficient TpU chain packing at the nano-inclusion–polymer interface. The corresponding extra free volume fraction Φ_{fv} can be calculated using eqn (2.5):[52]

$$\Phi_{fv} = 1 - \frac{\rho_{eff}}{\rho_{add}} \quad (2.5)$$

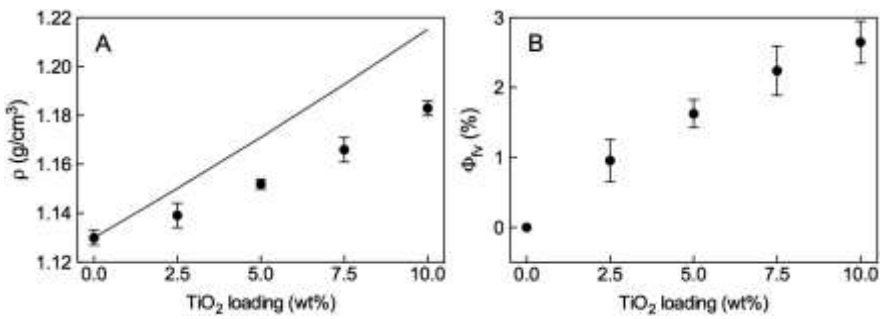

Figure 2.7 (A) Simulated additive (ρ_{add}) and effective (ρ_{add}) density values for TeG1000-MDI-bDo/Tio_2 nanocomposite membranes as a function of the nanoparticle concentration. Line: ρ_{add}; symbols: ρ_{eff}. Tio_2 simulated density = 3.46 g cm^{-3} (reported experimental values are in the range of 3.0–3.6 g cm^{-3}, depending on the fabrication method). (b) Free volume fraction for the system in panel (A) as calculated with eqn (2.5).

As shown in Figure 2.7(b), the presence of extra free volume resulting from the disturbed packing of the TpU polymer chain packing is confirmed by the positive values of Φ_{fv}, which increase with the increasing Tio_2 content. even if the calculated Φ_{fv} spans a limited range (between 0.96 and 2.65% for the case in Figure 2.7), its non-negligible value at each nanoparticle concentration can be taken as the underlying reason for the observed/simulated enhanced gas transport in all the TpU/Tio_2 nanocomposite membrane systems based on TeG1000 (as the soft phase),

MDI, and different chain extenders (eG, bDo, hDo, and DDo) studied in the present work.

2.4 Concluding Remarks

polymer nanocomposites are an area of substantial scientific interest and of emerging industrial application. Despite the proven benefits of nanocomposites, such as their mechanical and barrier properties and contribution to fire retardancy, polymer nanocomposites are used today only in niche applications. Thermoplastic polyurethanes are versatile materials displaying properties ranging from very soft thermoplastic elastomers to strong, rigid thermoplastics depending on their chemical composition, backbone structure, and resultant micro-phase morphology. The ennoblement of TpU by adding nanofillers to achieve better performing nanomaterials is even more difficult than for other polymeric matrices (*e.g.*, nylon or other thermoplastics), given the peculiar chemical nature and morphology of these macromolecules. In fact, while the alternating blocks and the variety of monomers used to synthesise the co-polymer structure allow tailoring of the properties of TpUs, these same characteristics play major roles in determining the ultimate macroscopic performance of the relevant nanocomposites, together with the specific properties of different nanofillers and the underlying nanocomposite production method. Since a heuristic approach to TpUnC design and production is excessively long and costly in economical and labour- intensive terms, further development of such nanomaterials depends on the fundamental understanding of their hierarchical structure and behaviour, which unavoidably requires multiscale modelling and simulation strategies to provide seamless coupling among various length and time scales. Accordingly, in this chapter, we have provided a multiscale molecular modelling recipe to achieve these goals and illustrated how such *in silico* techniques can be successfully employed to predict at least some of the major features and properties of polymer nanocomposites – with specific examples concerning TpUnCs – with a reliable degree of confidence.

Acknowledgements

This work was funded by the european Commission under the grant agreement number 604271 (project acronym: MoDena; project identifier: Fp7-nMp-2013-SMALL).

References

1. A . White, *MRS Bull.*, 2012, **37**, 715.
2. M . hermann, T. pentek and b. otto, *Proceedings of the 49th Hawaii International Conference on System Sciences (HICSS)*, koloa, hI, 2016, p. 3928, DoI: 10.1109/hICSS.2016.488.
3. p. k. Tewari, *Nanocomposite Membrane Technology: Fundamentals and Applications*, CRC press, boca Raton, 2015.
4. T . A. Saleh and V. k. Gupta, *Nanomaterial and Polymer Membranes, Synthesis, Characterization, and Applications*, elsevier, Amsterdam, 2016.

5. J . C. Charpentier, *Chem. Eng. Sci.*, 2002, **57**, 4667.
6. S . C. Glotzer and W. paul, *Annu. Rev. Mater. Res.*, 2002, **32**, 401.
7. Q . h. zeng, A. b. Yu and G. Q. Lu, *Prog. Polym. Sci.*, 2008, **33**, 191.
8. J . Jancar, J. F. Douglas, F. W. Starr, S. k. kumar, p. Cassgnau, A. J. Lesser, S. S. Sternstein and M. J. buehler, *Polymer*, 2010, **51**, 3321.
9. S . Yip, *Nat. Mater.*, 2003, **2**, 3.
10. S . Mohanty and R. Ross, in *Multiscale Simulation Methods for Nanomaterials*, ed. S. Mohanty and R. Ross, John Wiley & Sons, hoboken, 2008, p. 1.
11. G . Scocchi, p. posocco, J. W. handgraaf, J. G. e. M. Fraaije, M. Fermeglia and S. pricl, *Chem.–Eur. J.*, 2009, **15**, 7586.
12. S . pricl, p. posocco, G. Scocchi and M. Fermeglia, in *Handbook of Nanophysics: Functional Nanomaterials*, ed. k. D. Sattler, CRC press, boca Raton, 2010, pp. 3-1–3-15.
13. S . p. pereira, G. Scocchi, R. Toth, p. posocco, D. Romero-nieto, S. pricl and M. Fermeglia, *J. Multiscale Modell.*, 2011, **3**, 151.
14. R . Toth, F. Santese, S. p. pereira, D. R. nieto, S. pricl, M. Fermeglia and p. posocco, *J. Mater. Chem.*, 2012, **22**, 5398.
15. R . McWeeny, *Methods of Molecular Quantum Mechanics*, Academic press, Cambridge, 2nd edn, 1992.
16. A . F. de baas, *What Makes a Material Function? Let Me Compute the Ways*, european Commission, Directorate-General for Research and Innovation, Directorate D - Industrial Technologies, Unit D3-Advanced Materials and nanotechnologies, bruxelles, 2017, DoI: 10.2777/417118.
17. F . ercolessi and J. b. Adams, *Europhys. Lett.*, 1994, **26**, 583.
18. M . Fermeglia, M. Ferrone and S. pricl, *Fluid Phase Equilib.*, 2003, **212**, 315.
19. V . V. Aa, in *Molecular Simulations and Industrial Applications*, ed. k. e. Gubbins and n. Quirke, Gordon & breach, Amsterdam, 1996.
20. J . C. Chen and A. S. kim, *Adv. Colloid Interface Sci.*, 2004, **112**, 159.
21. p. J. hoogerbrugge and J. M. V. A. koelman, *Europhys. Lett.*, 1992, **19**, 155.
22. R . D. Groot and p. b. Warren, *J. Chem. Phys.*, 1997, **107**, 4423.
23. S . Chen and G. D. Doolen, *Annu. Rev. Fluid Mech.*, 1998, **30**, 329.
24. S . C. Glotzer, in *Annual Reviews of Computational Physics*, ed. D. Stauffer, World Scientific, Singapore, 1995, pp. 1–46.
25. J . G. e. M. Fraaije, b. A. C. van Vlimmeren, n. M. Maurits, M. postma, o. A. evers, C. hoffmann, p. Altevogt and G. Goldbeck-Wood, *J. Chem. Phys.*, 1997, **106**, 4260.
26. T . J. R. hughes, *The Finite Element Method*, prentice-hall, englewood Cliffs, 1987.
27. A . A. Gusev, *Macromolecules*, 2001, **34**, 3081.
28. W . A. Goddard III, T. Cagin, M. blanco, n. Vaidehi, S. Dasgupta, W. Floriano, M. belmares, J. kua, G. zamanakos, S. kashihara, M. Iotov and G. Gao, *Comput. Theor. Polym. Sci.*, 2011, **11**, 329.
29. S . McGrother, G. Goldbeck-Wood and Y. M. Lam, *Lect. Notes Phys.*, 2004, **642**, 223.
30. G . Scocchi, p. posocco, M. Fermeglia and S. pricl, *J. Phys. Chem. B*, 2007, **111**, 2143.

31. p. Cosoli, G. Scocchi, S. pricl and M. Fermeglia, *Microporous Mesoporous Mater.*, 2008, **107**, 169.
32. M . Fermeglia and S. pricl, *Comput. Chem. Eng.*, 2009, **33**, 1701.
33. M . Doi, *J. Comput. Appl. Math.*, 2002, **149**, 13.
34. G . Milano and F. Muller-plathe,¨ *J. Phys. Chem. B*, 2005, **109**, 18609.
35. R . Toth, D. J. Voorn, J. W. handgraaf, J. G. e. M. Fraaije, M. Fermeglia, S. pricl and p. posocco, *Macromolecules*, 2009, **42**, 8260.
36. A . Ghanbari, T. V. M. ndoro, F. Leroy, M. Rahimi, M. C. böhm and F. Muller-plathe,¨ *Macromolecules*, 2012, **45**, 572–584.
37. F . Muller-plathe,¨ *Chem. Phys. Chem.*, 2002, **3**, 754.
38. M . Fermeglia and S. pricl, *Prog. Org. Coat.*, 2007, **5**, 187.
39. b. Guo, z. Tang and L. zhang, *Prog. Polym. Sci.*, 2016, **62**, 29.
40. G . Choudalakis and A. D. Gotsis, *Curr. Opin. Colloid Interface Sci.*, 2012, **17**, 132.
41. h. Cong, M. Radosz, b. F. Towler and Y. Shen, *Sep. Purif. Technol.*, 2007, **55**, 281.
42. Y . kong, h. Du, J. Yang, D. Shi, Y. Wang, Y. zhang and W. Xin, *Desalination*, 2002, **146**, 49.
43. S . S. hosseini, Y. Li, T.-S. Chung and Y. Liu, *J. Membr. Sci.*, 2007, **302**, 207.
44. S . Matteucci, V. A. kusuma, S. D. kelman and b. D. Freeman, *Polymer*, 2008, **49**, 1659.
45. X . Liang, D. M. king, M. D. Groner, J. h. blackson, J. D. harris, S. M. George and A. W. Weimer, *J. Membr. Sci.*, 2008, **302**, 1057.
46. k. J. berean, J. z. ou, M. nour, M. R. Field, M. M. Y. A. Alsaif, Y. Wang, R. Ramanathan, V. bansal, S. kentish, C. M. Doherty, A. J. hill, C. McSweeney, R. b. kaner and k. kalantar-zahed, *J. Phys. Chem. C*, 2015, **119**, 13700.
47. M . Sadeghi, M. A. Semsarzadeh, M. barikani and b. Ghalei, *J. Membr. Sci.*, 2011, **385–386**, 76.
48. J . M. herrera-Alonso, e. Marand, J. C. Little and S. C. Cox, *J. Membr. Sci.*, 2009, **337**, 208.
49. M . Sadeghi, M. A. Semsarzadeh, M. barikani and M. p. Chenar, *J. Membr. Sci.*, 2011, **376**, 188.
50. A . khosravi, M. Sadeghi, h. z. babadkohi and M. M. Talakesh, *Ind. Eng. Chem. Res.*, 2014, **53**, 2011.
51. e. bet-moushoul, Y. Mansourpanah, kh. Farhadi and M. Tabatabei, *Chem. Eng. J.*, 2016, **283**, 29.
52. Y . Chen, R. Wang, J. zhou, h. Fan and b. Shi, *Polymer*, 2011, **52**, 1856.
53. M . barikani and M. barmar, *Iran. Polym. J.*, 1996, **5**, 231.
54. W .-h. Lin and T.-S. Chung, *J. Membr. Sci.*, 2001, **186**, 183.
55. e . Laurini, p. posocco, M. Fermeglia and S. pricl, *J. Comput. Sci.*, 2016, **15**, 24.
56. S . pricl and M. Fermeglia, *Chem. Eng. Commun.*, 2003, **190**, 1267.
57. M . Fermeglia, M. Ferrone and S. pricl, *Mol. Simul.*, 2004, **30**, 289.
58. R . Toth, A. Coslanich, M. Ferrone, M. Fermeglia, S. pricl, S. Miertus and e. Chiellini, *Polymer*, 2004, **45**, 8075.
59. R . Toth, M. Ferrone, S. Miertus, e. Chiellini, M. Fermeglia and S. pricl, *Biomacromolecules*, 2006, **7**, 1714.

60. M . Fermeglia, p. Cosoli, M. Ferrone, S. piccarolo, G. Mensitieri and S. pricl, *Polymer*, 2006, **47**, 5979.
61. M . Maly, p. posocco, S. pricl and M. Fermeglia, *Ind. Eng. Chem. Res.*, 2008, **47**, 5023.
62. p. posocco, z. posel, M. Fermeglia, M. Lisal and S. pricl, *J. Mater. Chem.*, 2010, **20**, 10511.
63. z. posel, p. posocco, M. Lisal, M. Fermeglia and S. pricl, *Soft Matter*, 2016, **12**, 3600.
64. R . W. baker, *Membrane Technology and Application*, Wiley & Sons, Chichester, 2004.
65. k. Golzar, S. Amjad-Iranagh, M. Amani and h. Modarress, *J. Membr. Sci.*, 2014, **451**, 117.
66. p . Winberg, k. DeSitter, C. Dotremont, S. Mullens, I. F. J. Vankelecom and F. h. J. Maurer, *Macromolecules*, 2005, **38**, 3776.
67. R . Mahajan and W. J. koros, *Polym. Eng. Sci.*, 2002, **42**, 1420.
68. k. Ghosal and b. D. Freeman, *Polym. Adv. Technol.*, 1994, **5**, 673.
69. S . Matteucci, V. kusuma, D. Sanders, S. Swinnea and b. D. Freeman, *J. Membr. Sci.*, 2008, **307**, 196.